24th COBEM - 2017

24th ABCM International Congress of Mechanical Engineering
December 3-8, 2017, Curitiba, PR, Brazil

COBEM-2017-0182
EFFECT OF THE FLOW MACRO-SCALE ON THE EFFECTIVE DRAG COEFFICIENT IN GAS-SOLID RISER FLOWS

Seyed Reza Amini Niaki
Joseph Mouallem
Norman Chavez
Gabriel J. S. Netzlaff
Christian C. Milioli
Fernando E. Milioli
Department of Mechanical Engineering, School of Engineering of São Carlos, University of São Paulo, 13566-590 São Carlos-SP, Brazil
r.amini@usp.br; josephmouallem@usp.br; normanchavez@usp.br; gabriel.netzlaff@usp.br; ccosta@sc.usp.br; milioli@sc.usp.br

Abstract. *Large scale simulation of gas-particle riser flows with two-fluid modeling, where gas and particulate are both treated as interpenetrating continuum phases, does require closure models to deal with sub grid filtered parameters such as effective stresses and interphase interactions. The topology of a riser flow comprises coherent structures of particulate that develop in a multitude of space and time scales, which are qualitatively well captured by the current two-fluid formulations. Quantitative accuracy, on the other hand, is still out of reach mostly due to the lack of more accurate sub-grid models. One among the sub-grid models that require enhancement is that for the effective interphase drag. Suitable models for the effective drag have been recently derived from results of highly resolved simulations with two-fluid modeling, which account for sub-grid flow heterogeneities, but disregard any macro-scale impact. In this work it is showed that, in addition to usual sub-grid filtered parameters, effective drag modeling also requires correlation to macro-scale effects. It is showed that the domain averages solid volume fraction and the domain average gas flow Reynolds number stand as relevant macro-scale parameters to be accounted for if higher modeling accuracy is pursued.*

Keywords: *Gas-particle flow, Two fluid model, Fluidization, Macro-scale, Effective drag, MFIX*

1 Introduction

Two-fluid models, where gas and particulate are both treated as interpenetrating continuum phases, are widely applied in large scale simulation of gas-particle riser flows (e.g. Anderson and Jackson, 1967; Gidaspow, 1994). The very heterogeneous riser flows comprise coherent structures of particulate that are continuously formed and dissipated in a multitude of space and time scales. The accurate capture of the macro-scale of this complex topology through large scale simulation can only be met if accurate models are available to properly describe sub-grid filtered parameters. Among those parameters are the effective stresses on both phases and interphase interactions like the effective interphase drag coefficient. The current state of the art does provide drag closures that allow for good qualitative large scale solutions of riser flows, but a generalized model allowing for quantitative accurate solutions is still missing. This article intends to be a contribution in that context, by providing new subsides for sub-grid modeling enhancement.

Gas-particulate interface drag is extensively addressed in literature. One reason for that is its driving force role in gas-solid fluidization. The current state of the art in drag correlation came as an evolution of various investigations mostly developed throughout the first half of the 20th century (see, for instance, Clift et al., 1978). One important early contribution was done by Schiller and Nauman (1933). They proposed an empirical correlation for the drag over individual spherical particles in laminar unidirectional fluid flows, a work that may be considered as a starting point for many current developments. Of course, Schiller-Nauman's correlation is not suited to the multi-particle very heterogeneous fluidized flows, which simultaneously comprise very dense regions closing to maximum packing up to very dilute regions where solid fractions tend to zero. In order to deal with this situation, different procedures have been proposed, both theoretical and empirical. A well accepted approach has been implemented by Gidaspow (1994), where Ergun's correlation (Ergun, 1952) is applied in dense regions while Wen and Yu's correlation (Wen and Yu, 1966) is applied in dilute regions. Different procedures have been proposed to smooth the discontinuity between the correlations as the flow goes from very dense to very dilute (Huilin and Gidaspow, 2003; Leboreiro et al., 2008). While very popular, Gidaspow's approach applied to simulations with two-fluid modeling renders quite excessive drag in riser flows. This is attributed to the fact that both Ergun's and Wen and Yu's correlations were generated from empirical data for homogeneous flows (gas flows through fixed beds of particulate for Ergun's, and liquid-particulate fluidized flows for Wen and Yu's).

Drag correlations for fluidized flows have also been generated from results of computational simulations. Hill et al. (2001) correlated a drag coefficient to the flow Reynolds number using predictions from Lattice-Boltzmann simulations applying random cubic distributions of particulate taken to the limit of maximum packing, where the fluid phase was resolved applying an incompressible Navier-Stokes formulation. Benyahia et al. (2006) adapted Hill et al.'s correlation to particulate concentrations and Reynolds numbers typical of riser flows. Drag correlations have also been developed from results of numerical direct simulations for the gas composed with Lagrangean simulations for the particulate. There is a considerable literature following that line (e.g. Sundaram and Collins, 1997; Wang et al., 2000; Zhou et al., 2001; Février et al., 2005; Fede and Simonin, 2006). A recent procedure to deal with the heterogeneity of fluidized flows is the so called energy minimization multi-scale model (EMMS) of Li and Kwauk (1994). In this model the micro-scale interactions between gas and particles, and the meso-scale interactions between clusters and surroundings, are both defined having in view the minimization of the energy required for the flow to develop. Simplified versions of such model have been used with success by different researchers (Yang et al., 2004; Lu et al., 2009; Benyahia, 2010). Another line of development of sub-grid filtered models is based on highly resolved simulations with microscopic two-fluid modeling (Agrawal et al., 2001; Andrews IV et al., 2005; Igci et al., 2008; Igci and Sundaresan, 2011a, b; Parmentier et al., 2012; Ozel et al., 2013; Milioli et al., 2013; Agrawal et al., 2013; Schneiderbauer and Pirker, 2014; Sarkar et al., 2016). In two-fluid modeling all the phases, no matter fluid or particulate, are treated as interpenetrating continua. Departing from available micro-scale closures, the highly resolved simulations provide meso-scale solutions over which filtering is performed to provide sub-grid filtered data for parameters such as the effective drag coefficient. At the current state of affairs, the effective drag coefficient is correlated to inside filter averaged parameters only, disregarding any effects of the outside flow topology.

All of the above procedures have been applied to account for drag in riser flows, which partially succeeded in various ad-hoc situations. No procedure has, however, achieved generalized suitability nor accuracy. In the present work the procedure for generating sub-grid effective drag models based on highly resolved simulations with microscopic two-fluid modeling is taken one step ahead, by investigating the relevance of macro-scale effects which were previously disregarded. The current literature available models do account for sub-grid flow heterogeneities, but disregard any macro-scale effects associated to the flow topology. In this work it is showed that, in addition to usual sub-grid filtered effects, effective drag modeling also requires correlation to the macro-scale topology of the flow. It is showed that the domain averages solid volume fraction and the domain average gas flow Reynolds number stand as relevant macro-scale parameters to be accounted for.

2 Methodology

The number of particles in gas particle flows is huge, making the description of the motion of all the particles virtually impractical. Two-fluid modeling is introduced as a means of overcoming such difficulty. In this approach the gas and particle phases are treated as interpenetrating continua (Anderson and Jackson, 1967; Gidaspow, 1994). The formulation is developed departing from a fixed control volume containing both phases, over which integral balances for mass, momentum and energy are performed. By applying Gauss and Leibniz theorems, the integral balances are turned into instantaneous differential equations and jump conditions. Finally, averaging operators are applied so that the continuum hypothesis holds for the interpenetrating phases.

2.1 Microscopic two-fluid model

Meso-scale structures, namely clusters and streamers, of sizes 10-100 particle diameters are present in dilute riser flows (Agrawal et al., 2001).To probe the behavior of the flow at even the smaller scales, the numerical integration of the two-fluid model conservative equations must be performed over sufficiently refined grids. Such fine grids, however, cannot be afforded in large scale simulations owing to computational limitations, and sub-grid closures are required so that coarser grids can be applied. Sub-grid closures can be generated by solving the two-fluid model under suitable microscopic closures, through the so called highly resolved simulations with microscopic two-fluid modeling (Agrawal et al., 2001). In this formulation the microscopic closures for the solid phase properties are provided by the kinetic theory of granular flows, which includes an equation for granular energy conservation (Lun et al., 1984; Gidaspow, 1994). This equation provides a granular temperature to which continuum properties for particulate phases are correlated. Also, the gas-solid interface interaction is frequently described as a drag effect of the gas over the solid phase, usually through empirical correlations such as that of Wen and Yu (1966). The microscopic two-fluid model is here partially presented in Tab. 1, emphasizing the closures of main interest in the present work.

Table 1. Microscopic two-fluid model.

Conservation equations of continuity and momentum for both phases

1) $$\frac{\partial}{\partial t}\left(\rho_g \varphi_g\right) + \nabla\cdot\left(\rho_g \varphi_g \boldsymbol{v}_g\right) = 0$$

2) $$\frac{\partial}{\partial t}\left(\rho_s \varphi_s\right) + \nabla\cdot\left(\rho_s \varphi_s \boldsymbol{v}_s\right) = 0$$

3) $$\frac{\partial}{\partial t}\left(\rho_g \varphi_g \boldsymbol{v}_g\right) + \nabla\cdot\left(\rho_g \varphi_g \boldsymbol{v}_g \boldsymbol{v}_g\right) = -\varphi_g \nabla\cdot\boldsymbol{\sigma}_g - \boldsymbol{M}_I + \rho_g \varphi_g \boldsymbol{g}$$

4) $$\frac{\partial}{\partial t}\left(\rho_s \varphi_s \boldsymbol{v}_s\right) + \nabla\cdot\left(\rho_s \varphi_s \boldsymbol{v}_s \boldsymbol{v}_s\right) = -\nabla\cdot\boldsymbol{\sigma}_s - \varphi_s \nabla\cdot\boldsymbol{\sigma}_g + \boldsymbol{M}_I + \rho_s \varphi_s \boldsymbol{g}$$

Volumetric continuity

5) $$\phi_s + \phi_g = 1$$

Conservation equation of granular (or pseudo-thermal) energy

6) $$\frac{3}{2}\left[\frac{\partial}{\partial t}\left(\rho_s \phi_s \Theta\right) + \nabla\cdot\left(\rho_s \phi_s \boldsymbol{v}_s \Theta\right)\right] = -\boldsymbol{\sigma}_s : \nabla \boldsymbol{v}_s + \nabla\cdot\left(\kappa_s \nabla\Theta\right) + \Gamma_{slip} - J_{coll} - J_{vis}$$

Closure for drag

7) $$\boldsymbol{M}_I = \beta\left(\boldsymbol{v}_g - \boldsymbol{v}_s\right)$$

8) $$\beta = \frac{3}{4} C_D \frac{\rho_g \varphi_s \varphi_g \left| \boldsymbol{v}_g - \boldsymbol{v}_s \right|}{\left(d_p \varepsilon_p\right)} \left(\varphi_g\right)^{-2.65}$$

9) $$C_D = \begin{cases} \dfrac{24}{\mathrm{Re}_p}\left(1 + 0.15\,\mathrm{Re}_p^{0.687}\right) & \text{for} \quad \mathrm{Re}_p < 1000 \\ 0.44 & \text{for} \quad \mathrm{Re}_p \geq 1000 \end{cases}$$

10) $$\mathrm{Re_p} = \frac{\left|\boldsymbol{v}_\mathrm{g} - \boldsymbol{v}_\mathrm{s}\right| \mathrm{d_p} \rho_\mathrm{g} \phi_\mathrm{g}}{\mu_\mathrm{g}}$$

Further closures may be found in Mouallem et al. (2017).

2.2 Filtered two-fluid model

This article analyses the behavior of a filtered parameter (effective drag) which is required as sub-grid closure in large scale simulations of riser flows using two-fluid filtered formulations. In order to make it clear how the effective drag is accounted for, the concerning filtered formulation is partially presented in Tab. 2, emphasizing the equations of main interest in the present work. The formulation in Tab. 2 is obtained by applying a volumetric filter over the microscopic model equations given in Tab. 1. The filtering procedure introduces new terms into the momentum equations in addition to those of the microscopic formulation. One such a term accounts for fluctuations on the buoyancy force exerted by the gas over the solid phase. This interface force is frequently added to the filtered drag force, defining an effective force usually referred to as effective drag owing to drag's predominance in gas-solid fluidized flows.

Table 2. Filtered two-fluid model.

Filtered continuity and momentum conservation equations

11) $$\frac{\partial}{\partial t}\left(\rho_g \bar{\varphi}_g\right) + \nabla\cdot\left(\rho_g \bar{\varphi}_g \tilde{\boldsymbol{v}}_g\right) = 0$$

12) $$\frac{\partial}{\partial t}\left(\rho_s \bar{\varphi}_s\right) + \nabla\cdot\left(\rho_s \bar{\varphi}_s \tilde{\boldsymbol{v}}_s\right) = 0$$

13) $$\frac{\partial}{\partial t}\left(\rho_\mathrm{g} \bar{\phi}_\mathrm{g} \tilde{\boldsymbol{v}}_\mathrm{g}\right) + \nabla\cdot\left(\rho_\mathrm{g} \bar{\phi}_\mathrm{g} \tilde{\boldsymbol{v}}_\mathrm{g} \tilde{\boldsymbol{v}}_\mathrm{g}\right) = -\bar{\phi}_\mathrm{g}\nabla\cdot\tilde{\boldsymbol{\sigma}}_\mathrm{g} - \nabla\cdot\boldsymbol{\tau}'_\mathrm{g} - \left(\boldsymbol{B}'_\mathrm{gs} + \overline{\boldsymbol{M}}_\mathrm{I}\right) + \rho_\mathrm{g}\bar{\phi}_\mathrm{g}\boldsymbol{g}$$

14) $$\frac{\partial}{\partial t}\left(\rho_\mathrm{s} \bar{\phi}_\mathrm{s} \tilde{\boldsymbol{v}}_\mathrm{s}\right) + \nabla\cdot\left(\rho_\mathrm{s} \bar{\phi}_\mathrm{s} \tilde{\boldsymbol{v}}_\mathrm{s} \tilde{\boldsymbol{v}}_\mathrm{s}\right) = -\nabla\cdot\bar{\boldsymbol{\sigma}}_\mathrm{s} - \nabla\cdot\boldsymbol{\tau}'_\mathrm{s} - \bar{\phi}_\mathrm{s}\nabla\cdot\tilde{\boldsymbol{\sigma}}_\mathrm{g} + \left(\boldsymbol{B}'_\mathrm{gs} + \overline{\boldsymbol{M}}_\mathrm{I}\right) + \rho_\mathrm{s}\bar{\phi}_\mathrm{s}\boldsymbol{g}$$

Filtered volumetric continuity

15) $$\bar{\phi}_s + \bar{\phi}_g = 1$$

Closure for effective drag

Filtered drag force

16) $$\overline{\boldsymbol{M}}_\mathrm{I} = \overline{\beta\left(\boldsymbol{v}_\mathrm{g} - \boldsymbol{v}_\mathrm{s}\right)}$$

Buoyancy fluctuation force (viscous terms are usually disregarded as lower order)

17) $$\boldsymbol{B}'_{gs} = -\left[\,\overline{\varphi_s \nabla\cdot\boldsymbol{\sigma}_g} - \bar{\varphi}_s \nabla\cdot\bar{\boldsymbol{\sigma}}_g\,\right] \approx -\left[\,\overline{\varphi_s \nabla P_g} - \bar{\varphi}_s \nabla \bar{P}_g\,\right]$$

Effective drag force

18) $$\beta_\mathrm{eff}\left(\tilde{\boldsymbol{v}}_\mathrm{g} - \tilde{\boldsymbol{v}}_\mathrm{s}\right) = \boldsymbol{B}'_\mathrm{gs} + \overline{\boldsymbol{M}}_\mathrm{I}$$

19) $$\beta_{eff} = \frac{\overline{\beta\left(\boldsymbol{v}_g - \boldsymbol{v}_s\right)}}{\left(\tilde{\boldsymbol{v}}_g - \tilde{\boldsymbol{v}}_s\right)} - \frac{\left[\,\overline{\varphi_s \nabla P_g} - \bar{\varphi}_s \nabla \bar{P}_g\,\right]}{\left(\tilde{\boldsymbol{v}}_g - \tilde{\boldsymbol{v}}_s\right)}$$

The drag coefficient correction is defined as:

20) $$\mathrm{H} = 1 - \frac{\beta_\mathrm{eff}}{\overline{\beta}}$$

Therefore, the effective drag force is calculated as:

21) $$\boldsymbol{B}'_\mathrm{gs} + \overline{\boldsymbol{M}}_\mathrm{I} = \left(1-\mathrm{H}\right)\overline{\beta}\left(\tilde{\boldsymbol{v}}_\mathrm{g} - \tilde{\boldsymbol{v}}_\mathrm{s}\right)$$

Further closures may be found in Mouallem et al. (2017).

2.3 Simulations and filtering

Highly resolved simulations were carried out for a typical fluid catalytic cracking particulate, under periodic boundary conditions. In all the simulations, particle diameter, particle density, gas density, and gas viscosity were set constant at 7.5×10^{-5} m, 1500 kg/m^3, 1.3 kg/m^3, 1.8×10^{-5} kg/(ms), respectively. The free fall terminal velocity and the particle Froude number of the concerning particulate are, respectively, 0.2184 m/s and 64.85.

A two-dimensional square domain of 16 cm x 16 cm was considered with a numerical mesh of 128 x 128 grids, so that a grid size of 1.25 mm x 1.25 mm was applied which provides grid size reasonably independent filtered results (Agrawal et al., 2001). Various average axial gas flow rates were enforced over the domain, and statistical steady state conditions were attained at various domain average gas Reynolds numbers. The domain average gas Reynolds number is defined as:

$$\left\langle \mathrm{Re}_g \right\rangle = \frac{\rho_g \left\langle \phi_g \right\rangle \left\langle \mathrm{v}_{g,y} \right\rangle \mathrm{d}_p}{\mu_g} \tag{22}$$

Domain average solid volume fractions $\langle \phi_s \rangle$ were imposed in different simulations (0.05, 0.15 and 0.25), covering a range relevant to rapid riser flows. The ratio between the domain average gas Reynolds number and its value under suspension conditions, $\left\langle \mathrm{Re}_g \right\rangle / \left\langle \mathrm{Re}_g \right\rangle_{susp}$, was set in a range covering flow conditions extending from fluidized suspensions up to topologies close to pneumatic transport (i.e. 1.0, 4.08, 8.15, 12.23, 16.30, 20.34 and 24.45). $\left\langle \mathrm{Re}_g \right\rangle_{susp}$ results from imposing a gas pressure gradient in the axial direction over the domain that exactly matches the gravity acting on the gas-solid mixtures, that is

$$\Delta P_g = Y_{length} . g \left[\rho_s \left\langle \phi_s \right\rangle + \rho_g \left\langle \phi_g \right\rangle \right] \tag{23}$$

Here $\left(Y_{length} \right)$ is the length of the domain in the axial direction.

The filtering procedure for deriving filtered data from results of highly resolved simulations is illustrated in "Fig 1. A" number of snapshots is considered inside the statistical steady state flow regime, through a given time interval which must be large enough so that robust statistics can be extracted. A square filter is defined comprising a number of grids, and made to sweep throughout the whole domain, collecting inside filter averages. In this process the collected averages are classified and further averaged inside bins defined by ranges of suitable independent variables (markers). In previous works the filtered solid volume fraction and the filtered slip velocity were identified as suitable markers for the effective drag coefficient (Milioli et al., 2013). In the current work storage is done over 64 x 80 bins, meaning 64 gaps of solid volume fraction (1st marker) and 80 gaps of filtered slip velocity (2nd marker).

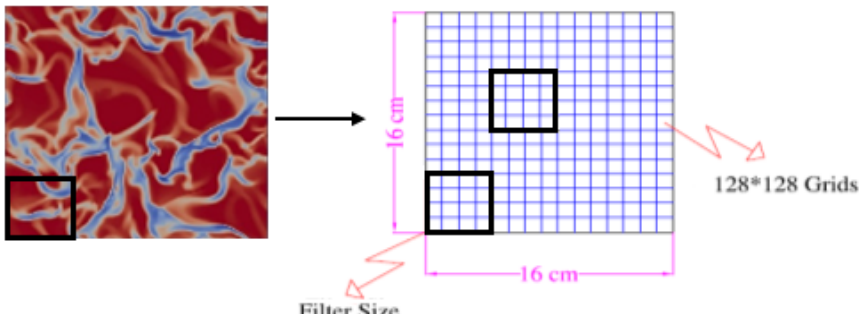

Figure 1. A. snapshot of solid volume fraction field and numerical grid from a typical 2D periodic simulation of a dilute gas-solid flow, showing a filtering window that sweeps through providing for average filtered data.

In this work all the simulations were done using MFIX, an open source code developed by NETL (National Energy Technology Laboratory, DOE-USA). The two-fluid model equations in MFIX are discretized through the finite volume method, and the resulting numerical code is solved through a point by point numerical technique. Comprehensive descriptions of MFIX modeling and numerical approaches can be found in Syamlal et al. (1993) and Syamlal (1998).

3 Results and discussion

Highly resolved simulations were performed for various cases of gas-solid fluidization under controlled domain average solid volume fractions and domain average gas Reynolds numbers, aiming to evaluate the effects of those macro-scale parameters over the effective drag coefficient correction. Filtering over the predictions, always performed inside the statistical steady state flow regime, provided for the desired effective drag coefficient correction. “Figure 2” illustrates how the statistical steady state flow regime is reached in a simulation departing from initial conditions of zero velocity fields for both the phases, for a particular case (suspension like conditions under a domain average solid volume fraction of 0.15). The graph shows how the domain average gas axial velocity changes in time until reaching a condition from where it keeps oscillating around a well stablished average, characterizing the beginning of the statistical steady state flow regime. In the considered case the statistical steady state regime was stablished after about 1s of real time flow simulation, a trend that also stands for all of the other cases considered here. In general, it was found that a time interval of 10s inside the statistical steady state regime was enough to provide robust statistics, for all the considered cases.

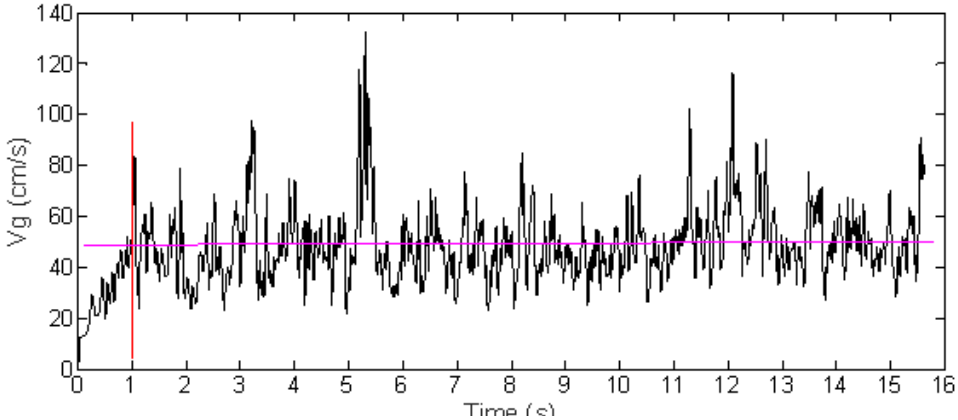

Figure 2. Transient behavior of the domain average gas phase axial velocity showing the establishment of the statistical steady state flow regime, for a simulation under suspension like conditions and an average solid volume fraction of 0.15.

Results for the drag coefficient correction *(H)*, are presented in “Fig 3” and “Fig 4” as a function of the filtered solid volume fraction ($\bar{\phi}_s$) and the dimensionless filtered axial slip velocity ($\tilde{v}_{slip,y}/v_t$), for various domain average solid volume fraction $\langle\phi_s\rangle$ and gas Reynolds number ratios $\langle Re_g\rangle/\langle Re_g\rangle_{susp}$. The results are presented for a unique dimensionless filter size ($\Delta_f/(v_t^2/g)=2.056$), corresponding to a 1 cm x 1 cm square box (results for other filter sizes may be found in Chavez-Cussy, 2017 and Mouallem et al., 2017). Both “Fig 3” and “Fig 4” show very significant effects of both $\langle\phi_s\rangle$ and $\langle Re_g\rangle/\langle Re_g\rangle_{susp}$ over (H). As seen in “Fig 3”, for all the considered $\langle\phi_s\rangle$ (0.05, 0.15 and 0.25), (H) varies significantly with $\langle Re_g\rangle/\langle Re_g\rangle_{susp}$. The effect of $\langle Re_g\rangle/\langle Re_g\rangle_{susp}$ over (H) is larger at smaller $(\bar{\phi}_s)$ and smaller $(\tilde{v}_{slip,y}/v_t)$. Also, the higher $\langle Re_g\rangle/\langle Re_g\rangle_{susp}$ the lower (H), showing that the flow becomes more homogeneous at higher gas Reynolds numbers (notice that (H) becomes much smaller at homogeneous conditions as Wen and Yu’s correlation becomes more suitable). Another feature observed in “Fig 3” is that the spread among the profiles of (H) for the various $\langle Re_g\rangle/\langle Re_g\rangle_{susp}$ becomes larger at smaller $(\tilde{v}_{slip,y}/v_t)$, an effect that becomes more prominent at smaller $(\bar{\phi}_s)$. It is seen that the effects of both, $\langle\phi_s\rangle$ and $\langle Re_g\rangle/\langle Re_g\rangle_{susp}$, become not significant at higher $(\tilde{v}_{slip,y}/v_t)$. It is also seen that, at any condition, $\langle Re_g\rangle/\langle Re_g\rangle_{susp}$ significantly affects (H) only as it grows above 8.15. The effects of the domain average solid volume fraction over the drag coefficient correction are more clearly seen in “Fig 4”. It is seen that the changes in (H) with

$\langle \phi_s \rangle$ are very small for $\langle \mathrm{Re}_g \rangle / \langle \mathrm{Re}_g \rangle_{susp}$ of 8.15 and bellow. For $\langle \mathrm{Re}_g \rangle / \langle \mathrm{Re}_g \rangle_{susp}$ above 8.15 there is a marked effect of $\langle \phi_s \rangle$ over (H), which grows higher the lower the filtered solid volume fraction $(\bar{\phi}_s)$.

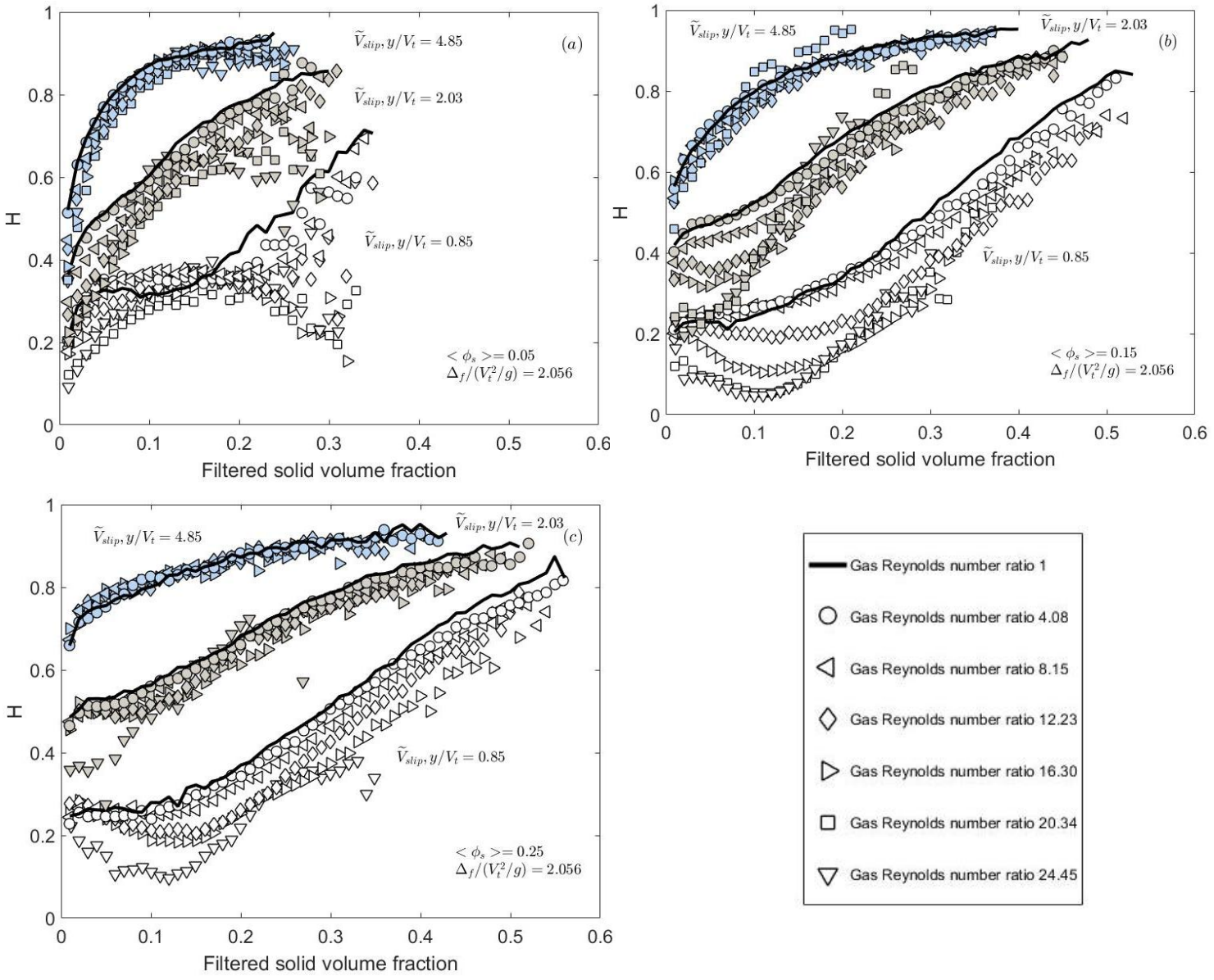

Figure 3. Drag coefficient correction (H), as a function of the filtered solid volume fraction $(\bar{\phi}_s)$ and the dimensionless filtered axial slip velocity $(\tilde{\mathrm{v}}_{slip,y}/\mathrm{v}_t)$, for various domain average solid volume fraction $\langle \phi_s \rangle$ and gas Reynolds number ratios $\langle \mathrm{Re}_g \rangle / \langle \mathrm{Re}_g \rangle_{susp}$. The results stand for a dimensionless filter size $\left(\Delta_\mathrm{f}/\left(\mathrm{v}_t^2/g\right) = 2.056\right)$.

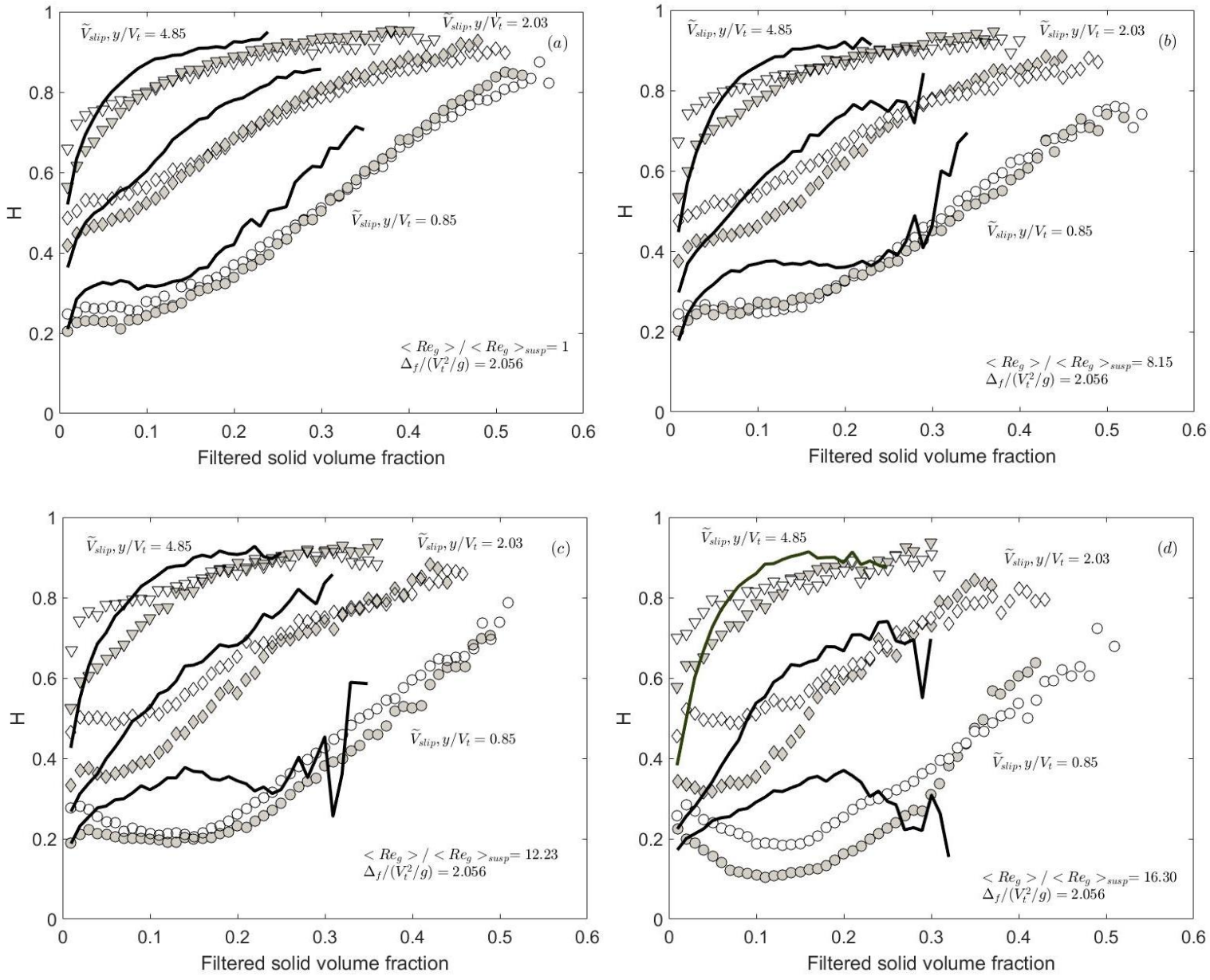

Figure 4. Drag coefficient correction (H), as a function of the filtered solid volume fraction ($\bar{\phi}_s$) and the dimensionless filtered axial slip velocity ($\tilde{v}_{slip,y}/v_t$), for domain average solid volume fraction $\langle \phi_s \rangle$ = 0.05 (black lines), 0.15 (gray symbols) and 0.25 (white symbols), and for gas Reynolds number ratios $\langle Re_g \rangle / \langle Re_g \rangle_{susp}$ = 1, 8.15, 12.23 and 16.30. The results stand for a dimensionless filter size ($\Delta_f/(v_t^2/g) = 2.056$).

4 Conclusion

This article advances an evaluation on the effects of macro-scale parameters associated to the flow topology on the effective drag in gas-solid riser flows. The macro-scale parameters of concern are the domain average solid volume fraction and the domain average gas Reynolds number. The analysis was performed using results of highly resolved simulations with microscopic two-fluid modeling. The simulations were carried out with the MFIX open source code, on 2D periodical

domains under specified average solid volume fractions and average gas flow Reynolds numbers. The predictions were filtered for successive snapshots taken inside the statistical steady state flow regime, applying space filters that were made to sweep all over the domain thereby collecting suitable statistics of relevant filtered parameters. Those filtered data were classified and stored as a function of suitable independent variables, namely the filtered solid volume fraction and the filtered slip velocity, following previous works. Results show that the effective drag, expressed as a drag coefficient correction, is considerably affected by both the domain average solid volume fraction and the domain average gas Reynolds number. This outcome points towards the necessity of accounting for those macro-scale parameters in sub-grid correlation of effective drag coefficients to be applied in large scale simulations of gas-solid riser flows.

5 Acknowledgements

This work was supported by The State of São Paulo Research Foundation (FAPESP), The National Council for Scientific and Technological Development (CNPq), and The Coordination for the Improvement of Higher Level Personnel (CAPES), all from Brazil.

Notation

$\boldsymbol{B}'$	fluctuation of gas-solid buoyancy force (Nm^{-3})
C_D	single particle drag coefficient (nd)
d_p	particle diameter (m)
$\boldsymbol{g}$, g	acceleration of gravity (ms^{-2})
H	drag coefficient correction (nd)
J_{coll}	rate of dissipation of granular energy by collisional damping ($Jm^{-3}s^{-1}$)
J_{vis}	rate of dissipation of granular energy by viscous damping ($Jm^{-3}s^{-1}$)
$\boldsymbol{M}$	drag force (Nm^{-3})
P	pressure (Nm^{-2})
Re_p	particle size based Reynolds number (nd)
t	time (s)
$\boldsymbol{v}$	velocity vector (ms^{-1})
y	vertical (axial) Cartesian coordinate (m)

Greek letters

β	micro-scale gas-solid drag coefficient ($kgm^{-3}s^{-1}$)
Γ_{slip}	rate of production of granular energy by gas-particle slip ($Jm^{-3}s^{-1}$)
Δ_f	filter size (m)
ε_p	particle sphericity (nd)
Θ	granular temperature (m^2s^{-2})
κ_s	granular thermal conductivity ($kgm^{-1}s^{-1}$)
ρ	density (kgm^{-3})
$\boldsymbol{\sigma}$	deviatoric stress tensor (Nm^{-2})
$\boldsymbol{\tau}'$	Reynolds like stress tensor (Nm^{-2})
ϕ	volume fraction (nd)

Subscripts

eff	effective, or meso-scale related
g	gas phase
I	interface
s	solid phase
$\overline{}$	filtered or volume average
~	Favre or mass weighed average, $\tilde{f} = \frac{\overline{\phi f}}{\overline{\phi}}$

6 References

Agrawal, K., Holloway, W., Milioli, C.C., Milioli, F.E. & Sundaresan, S., 2013, "Filtered models for scalar transport in gas-particle flows", Chem. Eng. Science, Vol,. 95, pp. 291-300.

Agrawal, K., Loezos, P.N., Syamlal, M. & Sundaresan, S., 2001, "The role of meso-scale structures in rapid gas-solid flows", J. Fluid Mech., Vol. 445, pp. 151-185.

Anderson, T.B. & Jackson, R., 1967, "Fluid Mechanical Description of Fluidized Beds. Equations of Motion", Indust. Engng. Chem. Fundam., Vol. 6, pp. 527-539.

Andrews IV, A.T., Loezos, P.N. & Sundaresan, S., 2005, "Coarse-grid simulation of gas-particle flows in vertical risers", Ind. Eng. Chem. Res., Vol. 44, No. 16, pp. 6022-6037.

Benyahia, S., 2010, "On the effect of subgrid drag closures", Ind. Eng. Chem. Res., Vol. 49, pp. 5122-5131.

Benyahia, S., Syamlal, M. & O'Brien, T., 2006, "Extension of Hill-Koch-Ladd drag correlation over all ranges of Reynolds number and solids volume fraction", Powder Technol., Vol. 162, pp. 166-174.

Clift, R., Grace, J.R. & Weber, M.E., 1978, "Bubbles, Drops, and Particles", Dover Publications Inc., Mineola, NY, 381p.

Ergun, S., 1952, "Fluid Flow through Packed Columns", Chem. Engng. Prog., Vol. 48, No. 2, pp 89-94.

Fede, P. & Simonin, O., 2006, "Numerical study of the subgrid fluid turbulence effects on the statistics of heavy collifing particles", Physics of Fluids, Vol. 18, 045103.

Février P., Simonin, O. & Squires, K.D., 2005, "Partitioning of particle velocities in gas-solid turbulent flows into a continuous field and a spatially uncorrelated random distribution: theoretical formalism and numerical study", J. Fluid Mech., Vol. 533, pp.1-46.

Gidaspow, D., 1994, "Multiphase Flow and Fluidization", Academic Press, San Diego, CA, 407p.

Hill, R.J., Koch, D.L. & Ladd, A.J.C., 2001, "Moderate-Reynolds-number flows inordered and random arrays of spheres", J. Fluid Mech., Vol. 448, pp. 243-278.

Huilin, L. & Gidaspow, D., 2003, "Hydrodynamic simulations of gas-solid flow in a riser", Ind. Eng. Chem. Res., Vol. 42, pp. 2390-2398.

Igci, Y. & Sundaresan, S., 2011a, "Constitutive models for filtered two-fluid models of fluidized gas-particle flows", Ind. Eng. Chem. Res., Vol. 50, pp. 13190-13201.

Igci, Y. & Sundaresan, S., 2011b, "Verification of filtered two-fluid models for gas-particle flows in risers", AIChE J., Vol. 57, pp. 2691-2707.

Igci, Y., Andrews IV, A.T., Sundaresan, S., Pannala, S. & O'Brien, T., 2008, "Filtered two-fluid models for fluidized gas-particle suspensions", AIChE Journal, Vol. 54, No. 6, pp. 1431-1448.

Leboreiro, J., Joseph, G.G. & Hrenya, C.M., 2008, "Revisiting the standard drag law for bubbling, gas-fluidized beds", Powder Technol., Vol. 183, pp. 385-400.

Li, J. & Kwauk, M., 1994, "Particle-fluid two-phase flow energy-minimization multi-scale method", Metallurgy Industry Press, Beijing.

Lu, B., Wang, W. & Li, J., 2009, "Search for a mesh-independent sub-grid model for CFD simulation of gas-solid riser flows", Chem. Eng. Sci., Vol. 64, pp. 3437-3447.

Lun, C.K.K., Savage, S.B., Jeffrey, D.J. & Chepurniy, N., 1984, "Kinetic Theories for Granular Flows: Inelastic Particles in Couette Flow and Singly Inelastic Particles in a General Flow Field", J. Fluid. Mech., Vol. 140, pp.223-256.

Milioli, C.C., Milioli, F.E., Holloway, W., Agrawal, K. & Sundaresan, S., 2013, "Filtered two-fluid models of fluidized gas-particle flows: New constitutive relations", AIChE J., Vol. 59, pp. 3265-3275.

Mouallem, J., Chavez-Cussy, N., Niaki, S.R.A., Milioli, C.C. & Milioli, F.E., 2017, "On the effects of the flow macro-scale over meso-scale filtered parameters in gas-solid riser flows", submitted to AIChE Journal.

Özel, A., Fede, P. & Simonin, O., 2013, "Development of filtered Euler–Euler two-phase model for circulating fluidised bed: High resolution simulation, formulation and a priori analyses", Int. J. Multiphase Flow, Vol. 55 . pp. 43-63.

Parmentier, J-F, Simonin O. & Delsart O., 2012, "A functional subgrid drift velocity model for filtered drag prediction in dense fluidized bed", AIChE J., Vol. 58, pp. 1084-1098.

Sarkar, A., Milioli, F.E., Ozarkar, S., Li, T., Sun, X. & Sundaresan, S., 2016, "Filtered sub-grid constitutive models for fluidized gas-particle flows constructed from 3-D simulations", Chemical Engineering Science, Vol. 152, pp. 443-456.

Schiller, L. & Neuman, A., 1933, Z. Ver. Deutsch. Ing., Vol. 77, p. 318.

Schneiderbauer, S. & Pirker, S., 2014, "Filtered and Heterogeneity-Based Subgrid Modifications for Gas–Solid Drag and Solid Stresses in Bubbling Fluidized Beds", AIChE J., Vol. 60, pp. 839-854.

Sundaram, S. & Collins, L.R., 1997. "Collision statistics in an isotropic particle-laden turbulent suspension. Part 1. Direct numerical simulations", J. Fluid Mech., Vol. 335, pp. 75-109.

Syamlal, M., 1998, "MFIX documentation numerical technique", DE-AC21-95MC31346 U.S. Department of Energy, EG&G Technical Services of West Virginia, Morgantown-WV, USA.

Syamlal, M., Rogers, W. & O'Brien, T. J., 1993, "Theory guide", MFIX documentation, Vol. 1, DOE/METEC-94/1004 NTIS/DE9400087, National Technical Information Service, Springfield, VA.

Wang, L.-P., Wexler, A.S. & Zhou, Y., 2000, "Statistical mechanical description and modelling of turbulent collision of inertial particles", J. Fluid Mech., Vol. 415, pp. 117-153.

Wen, C.Y. &Yu, Y.U., 1966, "Mechanics of fluidization", Chem. Engng. Prog. Symp. Series, Vol. 62, pp. 100-111.

Yang, N., Wang, W., Ge, W., Wang, L. & Li, J., 2004, "Simulation of heterogeneous structure in a circulating fluidized-bed riser by combining the two-fluid model with the EMMS approach", Ind. Eng. Chem. Res., Vol. 43, pp. 5548-5561.

Zhou, Y., Wexler, A.S. & Wang, L.-P., 2001, "Modelling turbulent collision of bidisperse inertial particles", J. Fluid Mech., Vol. 433, pp. 77-104.

7 Responsibility notice

The authors are the only responsible for the printed material included in this paper.